eIf2α-regulated translation modulates the early adhesion of mesenchymal-like cells

Alexia Caillier[1,2], Nadine Morin[1,2], Mathilde Lavigne[1,2], Jean-Philippe Lambert[1,2,4], Rachid Mazrouï[1,2,5], Jonathan Bergeman[3,§], and Marc-Étienne Huot[1,2,5,§]

1. Centre de Recherche sur le Cancer de l'Université Laval, Québec, QC, Canada
2. CHU de Québec Research Center CHU de Québec-Université Laval, Québec, QC, Canada
3. Institut de Recherches Cliniques de Montréal, Montréal, QC, Canada
4. Département de Médecine Moléculaire, Université Laval, Québec, QC, G1V 0A6, Canada
5. Département de Biologie moléculaire, biochimie médicale et pathologie, Université Laval, Québec, QC, Canada

Keywords: Epithelial-to-mesenchymal transition, adhesion, translational regulation, eukaryotic translation initiation factor, metastasis, cancer.

§ Correspondence to:

Marc-Étienne Huot, PhD (OCRID # 0000-0001-5155-5338)
Phone: 418-525-4444 x14552
Email: Marc-Etienne.Huot@crchudequebec.ulaval.ca

Jonathan Bergeman, PhD
Phone: 514-987-5500 x5706
Email: jonathan.bergeman@ircm.qc.ca

One sentence summary: Translation regulates mesenchymal cell adhesion

ABSTRACT

Cellular invasion is a complex process that requires several interdependent biological mechanisms, which are initiated by changes in adhesion that establish a morphology favorable for migration. Hence, the regulation of adhesion potential is a rate-limiting step in metastasis. Our previous work revealed that *de novo* translation is necessary to regulate the adhesion of mesenchymal-like cells; however, the underlying translational regulatory mechanism and the identity of newly synthesized proteins needed for the adhesion process remain unidentified. Here, we describe a translational regulatory mechanism that modulates mesenchymal cell adhesion. We observed a drastic decrease in translation during the initial phase of adhesion, followed by a reprogramming of the translatome, characterized by an orchestrated wave of mRNA translation that increases the expression of specific proteins involved in adhesion. We observed that phosphorylation of eukaryotic translation initiation factor 2 subunit alpha (eIF2α), which inhibits general translation initiation, was drastically increased at the beginning of cell adhesion. As adhesion progressed, the selective increase in the translation of adhesion-related mRNAs intensified as eIF2α phosphorylation gradually decreased over time in mensenchymal cells, but not in epithelial cells. Taken together, we have identified a translational regulatory mechanism specifically affecting the adhesion process of mesenchymal cells, as well as metastatic cells that have undergone epithelial-to-mesenchymal transition.

INTRODUCTION

The spread of cancer is a complex process that requires several interdependent biological mechanisms, such as those controlling proliferation, migration, invasion, and adhesion (Jiang et al., 2015). The majority (80–90%) of solid tumors originate from the epithelium (Coradini et al., 2011, Hinck and Nathke, 2014), which mainly relies on cell-cell adhesion structures to maintain tissue integrity, as this is a critical step in the metastatic initiation process (Jung et al., 2019). Hence, to disseminate from the primary tumor, cancer cells must first adapt to its morphological plasticity, then undergo a partial epithelial-to-mesenchymal transition (EMT) (Tyler and Tirosh, 2021, Mani et al., 2008). As epithelial cancer cells gain mesenchymal proprieties, they lose their cell-cell anchorage dependency, allowing detachment from the primary tumor, while increasing their migratory and adhesion capacities, enabling their invasion into distant tissues to form metastases (Bakir et al., 2020, Acloque et al., 2009). Achieving these finely orchestrated adaptations is critical for metastasis, which is associated with poor prognosis (Zhang and Weinberg, 2018). Therefore, understanding the molecular process driving these steps is essential to develop specific strategies that target the process in order to impair metastasis and improve patient prognosis.

In a previous study, we characterized the importance of mRNA translation during the early phases of the adhesion process in mesenchymal cells and metastatic cancer cell lines that had gained the ability to express mesenchymal markers through EMT (Bergeman et al., 2016). This mechanism was not observed in epithelial cells or non-metastatic cancer cell lines that retained epithelial morphology marker expression. This adhesion-related translation was spatiotemporally regulated, occurring during the early phases of adhesion and mainly restricted to spreading initiation centers (SICs) (Bergeman et al., 2016), which were initially described as transient structures that precede the formation of adhesion complexes and their maturation into focal adhesions (de Hoog et al., 2004). We reported the presence of polyadenylated mRNA, robust translational activity, and RNA-binding proteins known to modulate

mRNA translation within SICs suggesting that these structures act in adhesion-specific mRNA translation, sub-locally producing proteins needed for adhesion complex formation and maturation.

We also showed that impairing translation could inhibit mesenchymal cell adhesion (Bergeman et al., 2016). Indeed, the use of translation inhibitors greatly impaired the cells' capacity to adhere to different substrates, including plastic, extracellular matrix components, and cultured cell monolayers. This effect was also observed in highly metastatic cancer cell lines that had gone through EMT and expressed mesenchymal markers. Conversely, the adhesion capacities of minimally metastatic cancer cell lines, which mainly express epithelial markers, were not affected by translation inhibition. Moreover, this translational-dependent adhesion mechanism affected the ability of metastatic cells to achieve trans-endothelial invasion. Indeed, global translation inhibition decreased metastatic cell adhesion on an endothelial cell monolayer and trans-endothelial invasion (Bergeman et al., 2016).

Herein, we have discovered an early adhesion mechanism involving translational reprogramming of specific mRNAs and investigated their temporal synthesis during adhesion. We identify the eukaryotic translation initiation factor 2 subunit alpha (eIF2α) as a main regulator of translational reprogramming in mesenchymal cells and mesenchymal-like cancer cells. This work suggests that mesenchymal-like cells, including highly metastatic cancer cells, initiate their adhesion process by adapting their translational activity and selectively translating mRNAs coding for key proteins involved in adhesion complex formation and maturation to modulate their adhesion capacity.

RESULTS AND DISCUSSION

Translation dynamics during cellular adhesion

To further understand the role of translation during the adhesion process, we assessed its dynamics of translation in mesenchymal- and epithelial-like cells. We first performed puromycylation assays, in which cells were treated with puromycin at different time points during adhesion to quantify their *de novo* translation activity (Bergeman and Huot, 2017). As in our previous work (Bergeman et al., 2016), we used MRC-5 primary human fibroblasts as a representative mesenchymal-like cell line (Fig. 1A), and HeLa cells as a comparative epithelial-like line (Fig. 1B). As expected, we observed a significant decrease in translation activity in MRC-5 cells immediately after seeding, followed by an increase in translation as adhesion progressed (Fig. 1A). Conversely, we did not observed significant variations in translation throughout the HeLa adhesion process (Fig. 1B). The pattern of translational regulation in MRC-5 cells was confirmed by estimating active mRNA translation using polyribosomal profiling (Fig. S1A). Together, these results suggest that MRC-5 cells rely on a specific translational reprogramming mechanism during the initial adhesion phase, that could be shared by other mesenchymal cells.

To confirm that the translation dynamics observed during the adherence process of MRC-5 cells were not cell-type specific, but rather dependent on cell morphology, we next examined two cancer cell lines known for their distinctive morphology and invasiveness (Yue et al., 2016, Nieva et al., 2012, Sommers et al., 1994). We first tested the highly invasive MDA-MB-231 cell line, which expresses mesenchymal markers whose adhesion kinetics are affected by translation inhibition (Bergeman et al., 2016). In concordance with the mesenchymal cell line (MRC-5), MDA-MB-231 cells displayed a translational repression during the initial adhesion process, followed by gradual translational activation (Fig. 1C). As a control, we tested the MDA-MB-468 cell line, which expresses epithelial markers and is insensitive to translational inhibition (Bergeman et al., 2016). Like HeLa cells, we observed no variations in MDA-MB-468 cell translation during adhesion (Fig. 1D).

Collectively, our results corroborated the importance of regulated translational activity during mesenchymal cell adhesion (Bergeman et al., 2016) and suggested that contrary to epithelial-like cells, mesenchymal-like cells modulate their translatome throughout the process.

Phosphorylation of eIF2α in adhering mesenchymal cells adhesion

The observed translational regulation occuring in adhering mesenchymal cells seemed similar to the one observed in stress-induced translational reprogramming (Khong et al., 2017, Mokas et al., 2009). Following treatment with various type of stress, including oxydative (i.e., arsenite), endoplasmic reticulum (i.e. thapsigargin) or proteotoxic (i.e. proteasome inhibitor MG132), cells rapidly shutdown general translation initiation, through a mechanism involving the phosphorylation of eIF2α (Gordiyenko et al., 2019, Holcik, 2015). Concomitantly, phosphorylated eIF2α-mediated inhibition of general translation allows preferential translation of selected mRNAs, that encode for proteins promoting cell survival in response to stress (Mateju et al., 2020, Adjibade et al., 2015, Harding et al., 2000a). Whether mechanical or enzymatic cell resuspension is an aggressive process that induces a stress response and downstream phosphorylation of eIF2α remains unknown. Based on our results showing an mRNA translation inhibition throughout the cell suspension and adhesion initiation, we reasoned that this might be the case. To assess this hypothesis, we compared levels of eIF2α phosphorylation at different time points during mesenchymal-like cell adhesion. In both MRC-5 and MDA-MB-231 cells (Fig. 2A, left panels), we observed evident levels of eIF2α phosphorylation in the early stages of adhesion (0-60 minutes post seeding), which gradually decline as adhesion continued. This result suggests that cell suspension preceding adhesion induces phosphorylation of eIF2α. Hence, we compared the levels of phosphorylation in resuspended and adhering cells to levels of phosphorylated eIF2α in cells exposed to known stressors, such as arsenite and thapsigargin (Fig. S1B). While we can observe eIF2α phosphorylation in resuspended

cells, levels of phosphorylated eIF2α were significantly lower when compared to either arsenite- or thapsigargin-treated cells. These results indicate that resuspension induces a stress response associated with phosphorylation of eIF2α, although less drastic than the one induced by classical stressors. Consistently, we did not observe a significant induction of the mRNA encoding the heat shock stress protein (Hsp70) in suspended as compared to either adhered or adhering cells, further indicating that resuspension induces a moderate stress response that resulted in a subtle increase in phosphorylation of eIF2α (Fig. S1C). This phosphorylation of eIF2α occurring in resuspended cells is, however, significant as it prevents accumulation of polyribsomes, which culminates during the initiation of the adhesion process (20 min post-seeding) (Fig. S1D). Taken together, the regulated eIF2α phosphorylation correlated with the observed polyribosomal shutdown and puromycylation pattern observed in Figure 1 and the results presented in Figure S1. Indeed, as adhesion progress however, we observed a constant decline of eIF2α phosphorylation, which starts 40-60 min post-seeding (Fig. 2A), correlating with the partial and steady accumulation of polyribosomes after 40 minutes of adhesion (Fig. S1D). These results indicate that translation of at least a subset of mRNAs is resumed during the late stages of the adhesion process following the decrease in eIF2α phosphorylation. This corroborates with the increase in puromycylation which starts 60 min post-seeding (Figure 1A and 1C). Consistent with their lack of translational changes, we observed no variations in eIF2α phosphorylation during adhesion in either HeLa or MDA-MB-468 cells (Fig. 2A, right panels). These results suggest that the observed modulation of translatome in meshenchymal cells occurs through a eIF2α phosphorylation dependent mechanism in response to a physiological stress induced by their resuspension.

Phosphorylation of eIF2 α regulates adhesion-related translation

During the early steps of translation initiation, the inactive eIF2-GDP complex is converted through the action of eIF2B to the active eIF2-GTP-Met-tRNAi ternary complex competent for translation initiation

(Jackson et al., 2010). However, upon stress, induction of eIF2α phosphorylation results in the sequestration of eIF2B into the eIF2-GDP complex preventing its conversion to the ternary complex, impairing eIF2 complex formation and function (Holcik, 2015, Gordiyenko et al., 2019, Adomavicius et al., 2019). This can be circumvented by treating cells with the small molecule ISRIB, which causes eIF2B overactivation, enables eIF2 activation even when eIF2α is phosphorylated, therefore bypassing eIF2α phosphorylation induced translation inhibition (Zyryanova et al., 2021, Rabouw et al., 2019, Yamashita et al., 1989). Hence, we next treated both types of adhering mesenchymal cells (MRC-5 and MDA-MB-231 cells) with ISRIB to assess changes in their translational activity throughout the adhesion process. As shown by puromycin incorporation assays (Fig. 2B & C), ISRIB treatment abrogated the translational control normally observed in these cells (Fig 1A & C). These results further support that the adhesion related translational reprogramming observed in mesenchymal cell is controlled through eIF2α phosphorylation.

The inactivation of eIF2α is caused by the a single phosphorylation event on Ser 51, which is catalysed by 4 kinases (GCN2, HRI, PERK and PKR) (Koncha et al., 2021). General control non-derepressible-2 (GCN2) was shown to be activated by amino acid starvation or UV irradiation (Dokladal et al., 2021, Jiang and Wek, 2005, Sood et al., 2000), while heme-regulated inhibitor (HRI) activated in response to heme deprivation, oxidative and mitochondrial stress (Chen and London, 1995, Fessler et al., 2020, Guo et al., 2020, Ranu and London, 1979, Zhang et al., 2018), whereas PKR-like endoplasmic reticulum kinase (PERK) is activated in response to endoplasmic reticulum stress or UV irradiation (Popovic et al., 2021, Wu et al., 2002, Harding et al., 2000b). Finally, protein kinase activated by double-stranded RNA (PKR) is known to be activated by double-stranded RNA during viral infection (Zhang et al., 2021, Marchal et al., 2014, Riley and Weintraub, 1979). Our results described above indicating a role of eIF2α phosphorylation in the adhesion related translational reprogramming suggest a potential role of the

upstream kinases in the adhesion process. To our best knowledge, the role of either eIF2α phosphorylating-kinase in regulating adherence was never reported. Hence, we transduced MRC-5 and HeLa cells with short-hairpin RNA (shRNAs) against GCN2, HRI, and PERK, while we excluded PKR due to the shRNA delivery method (Fig. S2A–C). MRC-5 cells expressing shRNA against GCN2 (shGCN2) adhered slightly faster than MRC-5 cells expressing a non-targeted mammalian shRNA (shNT; Fig. S3A), while MRC-5 cells depleted of HRI or PERK adhered approximately three times faster than control cells (Fig. S3B–C).

In HeLa cells, shGCN2 expression did not significantly affect adhesion (Fig. S3D), and contrary to our observations in MRC-5 cells, shHRI and shPERK expression caused slight decreases in adhesion compared to shNT-expressing HeLa cells (Fig. S3E–F). These results revealed a novel role of the phosphorylating-stress kinase, namely HRI and PERK in regulating the adherence process of mesenchymal-like cells, involving eIF2α phosphorylation-mediated translational regulation.

Translational overactivation accelerates mesenchymal cell adhesion

Cycloheximide-induced translational repression decreases both the adhesion speed of MRC-5 cells and the total number of cells that adhere (Bergeman et al., 2016). Hence, we reasoned that forcing translation activity should positively affect the adhesion process. As expected, ISRIB potently accelerated adhesion in both MRC-5 and MDA-MB-231 cells (Fig. 2D). These results imply that bypassing early eIF2α phosphorylation overrides the translational regulatory adhesion mechanism specific to mesenchymal-like cells and cancer cells that have undergone EMT, forcing them to initiate adhesion more quickly. This is is consistent with our previous report of decreased adhesion kinetics after inhibiting translation (e.g., with cycloheximide) (Bergeman et al., 2016).

Identification of the adhesion-regulated translatome

The orchestrated inhibition and burst of translation observed in adhering mesenchymal-like cells and the involvement of phosphorylated eIF2α-mediated translational regulation suggest that *de novo* protein synthesis facilitates the adhesion of newly seeded cells. We hypothesized that while initial adhesion events rapidly halt ongoing general translation, it enable the residual active translation machinery to produce proteins essential for the formation of adhesion complexes and subsequently those needed for their maturation into focal adhesions. To investigate this, we identified proteins specifically translated 45 minutes post-seeding, at which point the largest increase in translation during adhesion was observed (Fig. 1A).

To specifically identify translationally activated mRNAs, we immunoprecipitated puromycinated peptides using an optimized protocol (Fig. 3A). We treated adhering MRC-5 cells with puromycin for the final 5 min of the 45 min adhesion period. Fully adhered MRC-5 cells (48 h post-seeding) were treated with puromycin for 5 min as a control. Puromycinated peptides were immunoprecipitated from both samples (Fig. 3B), and identified by mass spectrometry. Proteins were considered specifically translated in our adhering cells if they had three or more peptides with scores at least ten-fold higher than in the control in at least two biological triplicates. Using this method, we identified 47 proteins that were specifically synthesized in adhering cells, among which 33% are already known to be directly involved in focal complex formation, maturation, and anchoring to the forming actin cytoskeleton (Fig. 3C). These results indicate that the specific translation pattern observed in adhering mesenchymal-like cells is due to the redirection of the translational machinery toward transcripts encoding adhesion-related proteins.

Translational dynamics of adhesion-related proteins in mesenchymal cells

To validate the puromycin immunoprecipitation results and assess whether the specific translation of mRNAs encoding for adhesion proteins is unique to mesenchymal-like cells, we selected specifically

synthesized proteins with involvement in the adhesion process and explored their expression dynamics in adhering MRC-5 and HeLa cells (Fig. 4). In MRC-5 cells, we observed clear variations in protein levels (Fig. 4A, middle column). In most cases, adhesion proteins were barely detectable in unadhered cells and their expression increased gradually as adhesion was initiated (40–90 min) and consolidated (90–240 min). These protein expression variations were not observed in HeLa cells (Fig. 4A, left column), consistent with the absence of translational variations over time (Fig. 1A) and the previously demonstrated lack of effect translation inhibition has on adhesion in these cells (Bergeman et al., 2016). The translational regulation that occurs during adherence of MRC-5 cells seems to be restricted to the adhesion proteins identified in our immunoprecipitation experiments. Indeed, no translational variation was observed for the G3BP stress granule assembly factor 1 (G3BP1), an RNA-binding protein known to be involved in mRNA translational regulation (Somasekharan et al., 2020, Sahoo et al., 2018, Aulas et al., 2015), eventhough this protein is highly enrich in immature adhesion structures (Bergeman et al., 2016). To determine if the gradual expression pattern of adhesion proteins was regulated by eIF2α phosphorylation, we forced translation by pretreating MRC-5 cells with 0.2 μM ISRIB, thus bypassing eIF2α phosphorylation-mediated translational inhibition. ISRIB treatment completely disrupted the translation patterns of these proteins in MRC-5 cells (Fig. 4A, right column), providing a pausible explanation of the accelerated adhesion potential observed in these cells (Fig. 2D).

As translational alterations also affected cancer cells that had undergone EMT, we next examined the expression pattern of some of the identified proteins in adhering MDA-MB-231 cells (Fig. 4B). We observed a similar protein expression pattern to that seen in MRC-5 cells (Fig. 4B, middle column), which was completely lost in presence of ISRIB (Fig. 4B, right column). The slight discrepancy between the two mesenchymal cell lines (MRC-5 and MDA-MB-231) in regard to the protein expression, might be attributed to cell morphology, which influences the mechanism regulating adhesion protein synthesis. In

cell mostly expressing ephitelial marker, we only observed a slight change in protein expression during the adhesion. Indeed in epithelial-like MDA-MB-468 cancer cells, the expression pattern was largely similar to that observed in HeLa cells (Fig. 4B, left column). These results clearly show that eIF2α phosphorylation-dependent translational regulation of adhesion molecules is restricted to mesenchymal cells lines and is an important mechanism shaping their adhesion process.

Taken together, our results show that cells adopting a mesenchymal morphology can modulate their adhesion potential through *de novo* translation. In these cells, the resuspension-induced stress caused by their resuspension limits their adhesion due to the induction of eIF2-α phosphorylation, causing significant reduction in mRNA translation. While this mechanism is revealed by experimental manipulation, it seems that the same mechanism is taking place in metastatic cells that underwent EMT, suggesting that these cells could react in a similar fashion when submitted to the shear stress of the blood flow. In both cases, the eventual contact with a suitable support alleviates this transitional inhibition, allowing the reinitialization of translation and the synthesis of new adhesion protein. Interestingly, we previously showed that in mesenchymal cells and metastatic cancer cells that had proceeded through EMT, close to 80% of total translation was restricted to SICs during adhesion (Bergeman et al., 2016, de Hoog et al., 2004). This suggests that the identified adhesion proteins be locally translated within these dynamic structures and could be involved in the final decision to initiate the adhesion process and pusrue with cellular spreading. Indeed, SICs are located directly above maturing adhesion sites, which could allow them to serve as translational hubs that provide nascent adhesion complexes with the structural proteins needed for their maturation into focal adhesions. This would also explain why in these cells, no fluctuations were observed in the translation of G3BP1, an RNA-binding protein known to regulate the translation of bound mRNA. This RNA-binding protein spatiotemporal regulation of synthesized proteins was also observed during neuronal growth (Sahoo et al., 2018, Chen et al., 2014, Klein et al., 2013),

invadopode formation (Mardakheh et al., 2015), and stress response (Aulas et al., 2015). Future work will allow a better understanding of the mechanisms underlying the SIC-based spatiotemporal translation of specific mRNAs that enable the maturation of newly formed adhesion complexes into mature focal adhesions in mesenchymal cells and metastatic cancer cells.

MATERIALS AND METHODS

Cell culture

MRC-5, HeLa, and HEK 293T cells were cultured in Dulbecco's modified Eagle's medium (DMEM; D6429; Millipore Sigma, Darmstadt, Germany) supplemented with 10% fetal bovine serum (FBS; 12483020; Thermo Fisher Scientific, Waltham, MA, USA) and 0.1% Penicillin-Streptomycin (450-200-EL; Wisent, St-Bruno, QC, Canada). MDA-MB-231 and MDA-MB-468 cells were cultured in Leibovitz's L-15 medium (41300-039; Thermo Fisher Scientific,Waltham, MA, USA) supplemented with 10% FBS without CO_2 supplementation.

RT_PCR

RNA were extracted with Trizol (#15596-018, Invitrogen, Waltham, MA, USA), reverse transcription was performed with the M-MuLV reverse transcriptase (28025013, Thermo Fisher Scientific,Waltham, MA, USA). 187,5 ng of cDNAs were used for each PCR using Taq polymerase (E00007, Genescript, Piscataway, NJ, USA) with the following primers: HSP70 Forward 5' GCCCAAACCCAAAGTGGAAC 3', HSP70 Reverse 5' CGTGTTAATCCATGCCGTGC 3', β-Tubulin Forward 5' TTCCACCCTGAGCAACTTATC 3', and β-Tubulin Reverse 5' TCAACATTCAGGGCTCCATC 3'.

RNA interference

All shRNA were generated by ligation of oligos into AgeI and EcoRI of pLKO.1 (Addgene plasmid #8453; Addgene, Teddington, UK). Lower case sequences represent the targeted sequences.

GCN2 #2: 5′- CCGGgcctaactggtgaagaagtatCTCGAgatacttcttcaccagttaggcTTTTTG-3′;

GCN2 #3: 5′- CCGGccctaaagaactgtcgttaacCTCGAggttaacgacagttctttagggTTTTTG-3′;

HRI #3: 5′- CCGGgatctgaagccaagaaataCTCGAgtatttcttggcttcagatcTTTTTG-3′;

HRI #4: 5′- CCGGggaagaggacagagagcaaCTCGAgttgctctctgtcctcttccTTTTTG-3′;

PERK #5: 5′-CCGGgctgaaagatgaaagcacaCTCGAgctcgagtgtgctttcatctttcagcTTTTTG-3′;

PERK #1 5′-CCGGccaaactgattataggtaaCTCGAgttacctataatcagtttggTTTTTG-3′;

non-targeted controls 5′-CCGGgcgcgatagcgctaataatttCTCGAgaaattattagcgctatcgcgcTTTTTG-3′

Viral infection

We produced lentiviruses by transfecting HEK 293T cells with 50ug PEI, 6 µg of psPAX2 packaging plasmid (plasmid #12260; Addgene, Teddington, UK), 2 µg pMD2.G envelope plasmid (plasmid #12259; Addgene, Teddington, UK), and 12 µg of the pLJM1 vector for overexpression (plasmid #19319; Addgene, Teddington, UK) or 12ug of the pLKO vector for shRNAs (plasmid #8453; Addgene, Teddington, UK). After 16 h of transfection, the medium was changed and lentiviruses were collected and filtered through a 0.45-µm filter 24 h later. Viruses were added to cells in a 1:1 ratio with DMEM supplemented with 10% FBS with 8 µg/mL polybrene (H9268-5G; Millipore Sigma, Darmstadt, Germany). For MRC-5, cells were plated in a 6 well plate 24h prior to infection until confluency reached 75%. For HeLa, viruses were added to cells in suspension (200 000 cells in a 6 well plate). 24h post infection cells were selected with puromycin (PJ593; Bio Basic, Markham, ON, Canada) 0,75ug for MRC-5 and 2ug for HeLa for 48-72h.

Protein detection

Cells were extracted with Laemmli buffer (2% SDS, 2% β-mercaptoethanol, 20mM Tris ph 8.8, 10% Glycerol). For all cell lines, protein levels were quantified and normalized using the Bio-Rad RC DC™ Protein Assay (5000122 ; Bio Rad, Hercules, CA, USA), and amido black staining was performed on each membrane to confirm protein transfer uniformity. Equal amounts of proteins were resolved by sodium dodecyl sulfate (SDS)-polyacrylamide gel electrophoresis (PAGE) and immunoblotted. Immunoblotting was performed with polyclonal antibodies against vimentin (550513; BD Bioscience, San Jose, CA, USA), β-actin (8457; Cell Signaling Technology, Danvers, MA, USA). EIF2S1 (EIF2α; ab5369; Abcam, Cambridge, UK), EIF2S1 p-S51 (pEIF2α; ab32157; Abcam, Cambridge, UK), EIF2AK1 (HRI; 56484;

Novus Biologicals, Centennial, CO, USA), PERK (5683; Novus Biologicals, Centennial, CO, USA), GCN2 (ab134053; Abcam, Cambridge, UK), clathrin (P1663; Cell Signaling Technology, Danvers, MA, USA), fascin (54545; Cell Signaling Technology, Danvers, MA, USA), talin (MAB1676; Millipore Sigma, Darmstadt, Germany), tubulin (ab7291; Abcam, Cambridge, UK), annexin A1 (610067; BD Biosciences, San Jose, CA, USA), actinin (6487; Cell Signaling Technology, Danvers, MA, USA), myosin heavy chain 9 (MYH9; 3403; Cell Signaling Technology, Danvers, MA, USA), filamin (ab76289; Abcam, Cambridge, UK), cofilin (5175; Cell Signaling Technology, Danvers, MA, USA), profilin (3237; Cell Signaling Technology, Danvers, MA, USA), and integrins α5 (4705; Cell Signaling Technology, Danvers, MA, USA), α4 (8440; Cell Signaling Technology, Danvers, MA, USA), Hsp70 (C92F3A-5; Novus Biologicals, Centennial, CO, USA), and β3 (13166; Cell Signaling Technology, Danvers, MA, USA). Immunoreactive proteins were visualized with either goat anti-mouse (7076; Cell Signaling Technology, Danvers, MA, USA), goat anti-rabbit (7074; Cell Signaling Technology, Danvers, MA, USA) or TrueBlot anti-rabbit (Rockland Immunochemicals, Limerick, PA, USA) antibodies conjugated to horseradish peroxidase, and Western Lightning Plus Enhanced Chemiluminescence Substrate for Western Blotting (NEL104001EA; Perkin-Elmer, Waltham, MA, USA). Protein quantification was performed in ImageJ version 1.0 (US National Institutes of Health, Bethesda, MD, USA). G3BP1 were used as negative controls.

In vitro adhesion assays

Exponentially growing MRC-5 (n=3) and MDA-MB-231 (n=2) cells were detached using 0.025% trypsin with 0.1% ethylenediaminetetraacetic acid (EDTA), counted, and treated with either 0.2 µM ISRIB or 50 µg/mL cycloheximide. Control cells were left untreated. Samples were plated (HeLa: 15 000 cells/well, MRC-5: 25 000 cells/well, MDA-MB-468: 25 000 cells/well and MDA-MB-231: 50 000 cells/well) in 96-well Corning™ Stripwell™ Microplates (07-200-97 ; Fisher Scientific, Pittsburgh, PA, USA), and incubated at 37°C in 5% CO_2 for 10, 40, 60, 90, 120, 240, and 360 min (n = 7 per time point). Cells were

fixed with 3.7% formaldehyde for 15 min and nuclei were stained with DAPI (1 µg/mL). Fluorescence intensity was measured at excitation and emission wavelengths of 355 and 460 nm, respectively, using a Fluoroskan Ascent Microplate Fluorometer (5200110 ; Thermo Fisher Scientific, Waltham, MA, USA). Empty wells were used as controls for background subtraction.

Puromycin incorporation and immunoprecipitation assays

Exponentially growing cells were seeded in 100 mm plates (83.3902 ; Sarstedt, Newton, NC, USA) and incubated at 37°C in 5% CO_2 for 45 min. Five minute prior to the time point completion, plates were washed carefully with prewarmed (37°C) complete medium to remove all unattached cells and incubated for the last five minutes with a prewarm complete medium (37°C) added with 5 µg/mL puromycin. Plates were washed with PBS and cells were scraped in 1 mL of lysis buffer (1% SDS, 5 mM EDTA, and 1 mM dithiothreitol (DTT)). After heating at 98°C for 5 min, the lysate was clarified by centrifugation at 12,000 × *g* for 10 min. The supernatant was diluted with 9 mL cold PBS and free puromycin was removed by centrifugation using Macrosep 3 kDa centrifugal filters (Pall). Concentrated lysate was diluted in non-denaturing lysis buffer (10 mM Tris pH 7.4, 1 nM EDTA, 150 mM NaCl, 1% Triton X-100, and EDTA-free protease inhibitor cocktail (Roche, 11873580001). Puromycylated peptides were immunoprecipitated using the 12D10 anti-puromycin antibody (MABE343; Millipore) bound to protein A agarose beads (11719408001, Millipore Sigma, Darmstadt, Germany), as previously done (Carbonneau et al., 2016, Huot et al., 2009). Samples were stored at -80°C until their analysis.

MS data acquisition, analysis and archival

Peptide samples were analyzed at the Sherbrooke mass spectrometry core facility. Briefly, samples were loaded and separated using a Dionex Ultimate 3000 nanoHPLC system. 10 µL of the sample in

1% (v/v) formic acid was loaded with a constant flow of 4 µL/min onto a trap column (Acclaim PepMap100 C_{18} column, 0.3 mm id × 5 mm, Dionex Corporation, Sunnyvale, CA). Peptides were then eluted off to a PepMap C_{18} nano column (75 µm × 50 cm, Dionex Corporation, Sunnyvale, CA) with a linear gradient of 5–35% solvent B (90% acetonitrile with 0.1% formic acid) over a four hours gradient with a constant flow of 200 nL/min. Peptides were injected into an OrbiTrap QExactive mass spectrometer (Thermo Fischer Scientific, Waltham, MA, USA) using an EasySpray source. The voltage was set to 2.0 kV and the temperature of the column was set to 40°C. Acquisition of the full scan MS survey spectra (m/z 350–1600 was performed at a resolution of 70,000 using the accumulation of 1,000,000 ions. Peptides fragmented by collision-induced dissociation were selected on the ten highest intensities for from the preview scan. The normalized collision energy used was 35% and the resolution was set at 17,500 for 50,000 ions with a filling time set to a maximum of 250 ms for the full scans and 60 ms for the MS/MS scans. Unassigned charge states as well as singly, 7 and 8 charged species for the precursor ions were not analyzed, and a dynamic exclusion list was set to 500 entries over a retention time of 40 seconds under a 10 ppm mass window. The lock mass option was also enabled, and data acquisition was done using Xcalibur version 2.2 SP1.48. Protein identification and quantification were performed using the MaxQuant software package version 1.6.17.0 as described previously (Cox and Mann, 2008), with the protein database from UniProtKB (Homo sapiens, 29/01/2021, 77,027 entries). For protein identification, carbamidomethylation on cysteine was used as a fixed modification and methionine oxidation and protein N-terminal acetylation were used as variable modifications. The enzyme was set to trypsin/P (ie no cleavages on lysine or arginine before a proline), with up to two miscleavages allowed. The mass tolerance was 7 ppm for the precursor ions and 20 ppm for the fragment ions. All MS files were deposited at MassIVE (massive.ucsd.edu) and assigned the identified MSV000087439. They can be downloaded at ftp://MSV000087439@massive.ucsd.edu using the “MSV000087439_reviewer” and “adhesion” as the username and password, respectively, until the manuscript publication.

Polysome profiling

Polysomal profiling was performed on MRC-5 cells at different time points during adhesion. Cells were washed with PBS, then lysed in 1 mL polysomal extraction buffer (20 mM Tris pH 7.5, 150 mM NaCl, 1.25 mM $MgCl_2$, 5 U/mL RNase Inhibitor (M0314S; New England Biolabs, Ipswich, MA, USA), EDTA-free protease inhibitor cocktail, 1 mM DTT, and 1% Nonidet P-40) for 15 min on ice. Extracts were clarified by centrifugation at 12,000 × *g* for 20 min at 4°C. Cytoplasmic extracts were loaded on 15–55% (w/v) linear sucrose gradients for sedimentation by ultracentrifugation. The gradient was read at 260 nm to generate a continuous absorbance profile. The area under the curve of the polysome fraction was calculated and compared to the area under the curve of the pooled 40S, 60S, and 80S fractions.

Statistical analysis

The statistical analysis was performed using GraphPad Prism version 9.1.0 (GraphPad Software, San Diego, CA, USA). For Fig. 1 A-D, Fig. 2 A-C and Fig. S1, unpaired two-tailed t-tests were performed between all signals and the maximum signal. For Fig 2D, unpaired two-tailed t-tests were performed between all respective time points of the control and treated condition. For Fig S3, unpaired two-tailed t-tests were performed between all respective time points for both curves.

REFERENCES

ACLOQUE, H., ADAMS, M. S., FISHWICK, K., BRONNER-FRASER, M. & NIETO, M. A. 2009. Epithelial-mesenchymal transitions: the importance of changing cell state in development and disease. *J Clin Invest,* 119**,** 1438-49.

ADJIBADE, P., ST-SAUVEUR, V. G., QUEVILLON HUBERDEAU, M., FOURNIER, M. J., SAVARD, A., COUDERT, L., KHANDJIAN, E. W. & MAZROUI, R. 2015. Sorafenib, a multikinase inhibitor, induces formation of stress granules in hepatocarcinoma cells. *Oncotarget,* 6**,** 43927-43.

ADOMAVICIUS, T., GUAITA, M., ZHOU, Y., JENNINGS, M. D., LATIF, Z., ROSEMAN, A. M. & PAVITT, G. D. 2019. The structural basis of translational control by eIF2 phosphorylation. *Nat Commun,* 10**,** 2136.

AULAS, A., CARON, G., GKOGKAS, C. G., MOHAMED, N. V., DESTROISMAISONS, L., SONENBERG, N., LECLERC, N., PARKER, J. A. & VANDE VELDE, C. 2015. G3BP1 promotes stress-induced RNA granule interactions to preserve polyadenylated mRNA. *J Cell Biol,* 209**,** 73-84.

BAKIR, B., CHIARELLA, A. M., PITARRESI, J. R. & RUSTGI, A. K. 2020. EMT, MET, Plasticity, and Tumor Metastasis. *Trends Cell Biol,* 30**,** 764-776.

BERGEMAN, J., CAILLIER, A., HOULE, F., GAGNE, L. M. & HUOT, M. E. 2016. Localized translation regulates cell adhesion and transendothelial migration. *J Cell Sci,* 129**,** 4105-4117.

BERGEMAN, J. & HUOT, M. E. 2017. Quantitative Immunofluorescence to Measure Global Localized Translation. *J Vis Exp*.

CARBONNEAU, M., L, M. G., LALONDE, M. E., GERMAIN, M. A., MOTORINA, A., GUIOT, M. C., SECCO, B., VINCENT, E. E., TUMBER, A., HULEA, L., BERGEMAN, J., OPPERMANN, U., JONES, R. G., LAPLANTE, M., TOPISIROVIC, I., PETRECCA, K., HUOT, M. E. & MALLETTE, F. A. 2016. The oncometabolite 2-hydroxyglutarate activates the mTOR signalling pathway. *Nat Commun,* 7**,** 12700.

CHEN, E., SHARMA, M. R., SHI, X., AGRAWAL, R. K. & JOSEPH, S. 2014. Fragile X mental retardation protein regulates translation by binding directly to the ribosome. *Mol Cell,* 54**,** 407-417.

CHEN, J. J. & LONDON, I. M. 1995. Regulation of protein synthesis by heme-regulated eIF-2 alpha kinase. *Trends Biochem Sci,* 20**,** 105-8.

CORADINI, D., CASARSA, C. & ORIANA, S. 2011. Epithelial cell polarity and tumorigenesis: new perspectives for cancer detection and treatment. *Acta Pharmacol Sin,* 32**,** 552-64.

COX, J. & MANN, M. 2008. MaxQuant enables high peptide identification rates, individualized p.p.b.-range mass accuracies and proteome-wide protein quantification. *Nat Biotechnol,* 26**,** 1367-72.

DE HOOG, C. L., FOSTER, L. J. & MANN, M. 2004. RNA and RNA binding proteins participate in early stages of cell spreading through spreading initiation centers. *Cell,* 117**,** 649-62.

DOKLADAL, L., STUMPE, M., PILLET, B., HU, Z., GARCIA OSUNA, G. M., KRESSLER, D., DENGJEL, J. & DE VIRGILIO, C. 2021. Global phosphoproteomics pinpoints uncharted Gcn2-mediated mechanisms of translational control. *Mol Cell,* 81**,** 1879-1889 e6.

FESSLER, E., ECKL, E. M., SCHMITT, S., MANCILLA, I. A., MEYER-BENDER, M. F., HANF, M., PHILIPPOU-MASSIER, J., KREBS, S., ZISCHKA, H. & JAE, L. T. 2020. A pathway coordinated by DELE1 relays mitochondrial stress to the cytosol. *Nature,* 579**,** 433-437.

GORDIYENKO, Y., LLACER, J. L. & RAMAKRISHNAN, V. 2019. Structural basis for the inhibition of translation through eIF2alpha phosphorylation. *Nat Commun,* 10**,** 2640.

GUO, X., AVILES, G., LIU, Y., TIAN, R., UNGER, B. A., LIN, Y. T., WIITA, A. P., XU, K., CORREIA, M. A. & KAMPMANN, M. 2020. Mitochondrial stress is relayed to the cytosol by an OMA1-DELE1-HRI pathway. *Nature,* 579**,** 427-432.

HARDING, H. P., NOVOA, I., ZHANG, Y., ZENG, H., WEK, R., SCHAPIRA, M. & RON, D. 2000a. Regulated translation initiation controls stress-induced gene expression in mammalian cells. *Mol Cell,* 6**,** 1099-108.

HARDING, H. P., ZHANG, Y., BERTOLOTTI, A., ZENG, H. & RON, D. 2000b. Perk is essential for translational regulation and cell survival during the unfolded protein response. *Mol Cell,* 5**,** 897-904.

HINCK, L. & NATHKE, I. 2014. Changes in cell and tissue organization in cancer of the breast and colon. *Curr Opin Cell Biol,* 26**,** 87-95.

HOLCIK, M. 2015. Could the eIF2alpha-Independent Translation Be the Achilles Heel of Cancer? *Front Oncol,* 5**,** 264.

HUOT, M. E., VOGEL, G. & RICHARD, S. 2009. Identification of a Sam68 ribonucleoprotein complex regulated by epidermal growth factor. *J Biol Chem,* 284**,** 31903-13.

JACKSON, R. J., HELLEN, C. U. & PESTOVA, T. V. 2010. The mechanism of eukaryotic translation initiation and principles of its regulation. *Nat Rev Mol Cell Biol,* 11**,** 113-27.

JIANG, H. Y. & WEK, R. C. 2005. GCN2 phosphorylation of eIF2alpha activates NF-kappaB in response to UV irradiation. *Biochem J,* 385**,** 371-80.

JIANG, W. G., SANDERS, A. J., KATOH, M., UNGEFROREN, H., GIESELER, F., PRINCE, M., THOMPSON, S. K., ZOLLO, M., SPANO, D., DHAWAN, P., SLIVA, D., SUBBARAYAN, P. R., SARKAR, M., HONOKI, K., FUJII, H., GEORGAKILAS, A. G., AMEDEI, A., NICCOLAI, E., AMIN, A., ASHRAF, S. S., YE, L., HELFERICH, W. G., YANG, X., BOOSANI, C. S., GUHA, G., CIRIOLO, M. R., AQUILANO, K., CHEN, S., AZMI, A. S., KEITH, W. N., BILSLAND, A., BHAKTA, D., HALICKA, D., NOWSHEEN, S., PANTANO, F. & SANTINI, D. 2015. Tissue invasion and metastasis: Molecular, biological and clinical perspectives. *Semin Cancer Biol,* 35 Suppl**,** S244-S275.

JUNG, H. Y., FATTET, L., TSAI, J. H., KAJIMOTO, T., CHANG, Q., NEWTON, A. C. & YANG, J. 2019. Apical-basal polarity inhibits epithelial-mesenchymal transition and tumour metastasis by PAR-complex-mediated SNAI1 degradation. *Nat Cell Biol,* 21**,** 359-371.

KHONG, A., MATHENY, T., JAIN, S., MITCHELL, S. F., WHEELER, J. R. & PARKER, R. 2017. The Stress Granule Transcriptome Reveals Principles of mRNA Accumulation in Stress Granules. *Mol Cell,* 68**,** 808-820 e5.

KLEIN, M. E., YOUNTS, T. J., CASTILLO, P. E. & JORDAN, B. A. 2013. RNA-binding protein Sam68 controls synapse number and local beta-actin mRNA metabolism in dendrites. *Proc Natl Acad Sci U S A,* 110**,** 3125-30.

KONCHA, R. R., RAMACHANDRAN, G., SEPURI, N. B. V. & RAMAIAH, K. V. A. 2021. CCCP-induced mitochondrial dysfunction - characterization and analysis of integrated stress response to cellular signaling and homeostasis. *FEBS J.*

MANI, S. A., GUO, W., LIAO, M. J., EATON, E. N., AYYANAN, A., ZHOU, A. Y., BROOKS, M., REINHARD, F., ZHANG, C. C., SHIPITSIN, M., CAMPBELL, L. L., POLYAK, K., BRISKEN, C., YANG, J. & WEINBERG, R. A. 2008. The epithelial-mesenchymal transition generates cells with properties of stem cells. *Cell,* 133**,** 704-15.

MARCHAL, J. A., LOPEZ, G. J., PERAN, M., COMINO, A., DELGADO, J. R., GARCIA-GARCIA, J. A., CONDE, V., ARANDA, F. M., RIVAS, C., ESTEBAN, M. & GARCIA, M. A. 2014. The impact of PKR activation: from neurodegeneration to cancer. *FASEB J,* 28**,** 1965-74.

MARDAKHEH, F. K., PAUL, A., KUMPER, S., SADOK, A., PATERSON, H., MCCARTHY, A., YUAN, Y. & MARSHALL, C. J. 2015. Global Analysis of mRNA, Translation, and Protein Localization: Local Translation Is a Key Regulator of Cell Protrusions. *Dev Cell,* 35**,** 344-57.

MATEJU, D., EICHENBERGER, B., VOIGT, F., EGLINGER, J., ROTH, G. & CHAO, J. A. 2020. Single-Molecule Imaging Reveals Translation of mRNAs Localized to Stress Granules. *Cell,* 183**,** 1801-1812 e13.

MOKAS, S., MILLS, J. R., GARREAU, C., FOURNIER, M. J., ROBERT, F., ARYA, P., KAUFMAN, R. J., PELLETIER, J. & MAZROUI, R. 2009. Uncoupling stress granule assembly and translation initiation inhibition. *Mol Biol Cell,* 20**,** 2673-83.

NIEVA, C., MARRO, M., SANTANA-CODINA, N., RAO, S., PETROV, D. & SIERRA, A. 2012. The lipid phenotype of breast cancer cells characterized by Raman microspectroscopy: towards a stratification of malignancy. *PLoS One,* 7**,** e46456.

POPOVIC, R., CELARDO, I., YU, Y., COSTA, A. C., LOH, S. H. Y. & MARTINS, L. M. 2021. Combined Transcriptomic and Proteomic Analysis of Perk Toxicity Pathways. *Int J Mol Sci,* 22.

RABOUW, H. H., LANGEREIS, M. A., ANAND, A. A., VISSER, L. J., DE GROOT, R. J., WALTER, P. & VAN KUPPEVELD, F. J. M. 2019. Small molecule ISRIB suppresses the integrated stress response within a defined window of activation. *Proc Natl Acad Sci U S A,* 116**,** 2097-2102.

RANU, R. S. & LONDON, I. M. 1979. Regulation of protein synthesis in rabbit reticulocyte lysates: additional initiation factor required for formation of ternary complex (eIF-2.GTP.Met-tRNAf) and demonstration of inhibitory effect of heme-regulated protein kinase. *Proc Natl Acad Sci U S A,* 76**,** 1079-83.

RILEY, D. & WEINTRAUB, H. 1979. Conservative segregation of parental histones during replication in the presence of cycloheximide. *Proc Natl Acad Sci U S A,* 76**,** 328-32.

SAHOO, P. K., LEE, S. J., JAISWAL, P. B., ALBER, S., KAR, A. N., MILLER-RANDOLPH, S., TAYLOR, E. E., SMITH, T., SINGH, B., HO, T. S., URISMAN, A., CHAND, S., PENA, E. A., BURLINGAME, A. L., WOOLF, C. J., FAINZILBER, M., ENGLISH, A. W. & TWISS, J. L. 2018. Axonal G3BP1 stress granule protein limits axonal mRNA translation and nerve regeneration. *Nat Commun,* 9**,** 3358.

SOMASEKHARAN, S. P., ZHANG, F., SAXENA, N., HUANG, J. N., KUO, I. C., LOW, C., BELL, R., ADOMAT, H., STOYNOV, N., FOSTER, L., GLEAVE, M. & SORENSEN, P. H. 2020. G3BP1-linked mRNA partitioning supports selective protein synthesis in response to oxidative stress. *Nucleic Acids Res,* 48**,** 6855-6873.

SOMMERS, C. L., BYERS, S. W., THOMPSON, E. W., TORRI, J. A. & GELMANN, E. P. 1994. Differentiation state and invasiveness of human breast cancer cell lines. *Breast Cancer Res Treat,* 31**,** 325-35.

SOOD, R., PORTER, A. C., OLSEN, D. A., CAVENER, D. R. & WEK, R. C. 2000. A mammalian homologue of GCN2 protein kinase important for translational control by phosphorylation of eukaryotic initiation factor-2alpha. *Genetics,* 154**,** 787-801.

TYLER, M. & TIROSH, I. 2021. Decoupling epithelial-mesenchymal transitions from stromal profiles by integrative expression analysis. *Nat Commun,* 12**,** 2592.

WU, S., HU, Y., WANG, J. L., CHATTERJEE, M., SHI, Y. & KAUFMAN, R. J. 2002. Ultraviolet light inhibits translation through activation of the unfolded protein response kinase PERK in the lumen of the endoplasmic reticulum. *J Biol Chem,* 277**,** 18077-83.

YAMASHITA, H., NOGUCHI, S., MURAKAMI, N., ADACHI, M., KATO, R., KATO, S., ISHIMATSU, T., NAKAYAMA, I., MANNEN, K., MIFUNE, K. & ET AL. 1989. Induction of peroxidase and thyroglobulin by TSH in cultured thyroid cells from patients with Basedow's disease and its inhibition by actinomycin D. *Acta Pathol Jpn,* 39**,** 121-6.

YUE, X., ZHAO, Y., ZHANG, C., LI, J., LIU, Z., LIU, J. & HU, W. 2016. Leukemia inhibitory factor promotes EMT through STAT3-dependent miR-21 induction. *Oncotarget,* 7**,** 3777-90.

ZHANG, S., MACIAS-GARCIA, A., VELAZQUEZ, J., PALTRINIERI, E., KAUFMAN, R. J. & CHEN, J. J. 2018. HRI coordinates translation by eIF2alphaP and mTORC1 to mitigate ineffective erythropoiesis in mice during iron deficiency. *Blood,* 131**,** 450-461.

ZHANG, W., LIU, Y., MIN CHIN, J. & PHUA, K. K. L. 2021. Sustained release of PKR inhibitor C16 from mesoporous silica nanoparticles significantly enhances mRNA translation and anti-tumor vaccination. *Eur J Pharm Biopharm,* 163**,** 179-187.

ZHANG, Y. & WEINBERG, R. A. 2018. Epithelial-to-mesenchymal transition in cancer: complexity and opportunities. *Front Med,* 12**,** 361-373.

ZYRYANOVA, A. F., KASHIWAGI, K., RATO, C., HARDING, H. P., CRESPILLO-CASADO, A., PERERA, L. A., SAKAMOTO, A., NISHIMOTO, M., YONEMOCHI, M., SHIROUZU, M., ITO, T. & RON, D. 2021. ISRIB Blunts the Integrated Stress Response by Allosterically Antagonising the Inhibitory Effect of Phosphorylated eIF2 on eIF2B. *Mol Cell,* 81**,** 88-103 e6.

Acknowledgments: We thank Drs. Josée N. Lavoie and François Bordeleau for sharing reagents. We thank High-Fidelity Science Communications for manuscript editing.

Financial support: This study was supported by grants from the Natural Sciences and Engineering Research Council of Canada (NSERC; RGPIN-2019-06494 to M.-E.H.; MOP-CG095386 to R.M.). A.C. is the recipient of a Ph.D. studentship from the Fonds de Recherche du Québec – Santé (FRQS). N.M. is the recipient of MSc studentships from NSERC and the Fonds de Recherche du Québec – Nature et Technologie. J.B. is the recipient of a postdoctoral fellowship from the FRQS.

Author contributions: A.C., J.B., and M.-E.H. designed the study. A.C. performed most of the experiments, with help from N.M., M.L. and J.B., who also optimized and performed the puromycin immunoprecipitation assay and polysome profiling. J.-P.L. and J.B. analyzed the mass spectrometry data. A.C. and M.-E.H. wrote the paper. All the authors discussed the results and commented on the manuscript at all the stages.

Competing interests: The authors declare no competing financial interests.

FIGURE LEGENDS

Fig. 1. Translational dynamics during cellular adhesion

Puromycin incorporation within actively synthetized polypeptides (5 μg/mL puromycin / 5 min) in (**A**) MRC-5, (**B**) HeLa, (**C**) MDA-MB-231, and (**D**) MDA-MB-468 cells. Puromycilation was revealed using an anti-purimycin specific antibody. Graphical representations (right panels) show the puromycin signals (middle panels) over the normalized amido black signals (left panels). Assays were performed in triplicate. Error bars represent the standard deviation. n.s., $p > 0.05$; *, $p \leq 0.05$; **, $p \leq 0.01$; ***, $p \leq 0.001$; ****, $p \leq 0.0001$ by two-tailed *t*-test.

Fig. 2. Phosphorylation of eIF2α during cellular adhesion

(**A**) Quantification of phosphorylated eIF2α normalized to total eIF2α during the adhesion of MRC-5, MDA-MB-231, HeLa, and MDA-MB-468 cells (n=3 for each cell line).

(**B**) Puromycilation assays (5 μg/mL puromycin / 5 min) on MRC-5 cells pretreated with 0.2 μM ISRIB (30 min). Graphical representations (right panels) show the puromycin signals (middle panels) over the normalized amido black signals (left panels). Assays were performed in triplicate.

(**C**) Puromycilation assays (5 μg/mL puromycin / 5 min) on MDA-MB-231 cells pretreated with 0.2 μM ISRIB (30 min). Graphical representations (right panels) show the puromycin signals (middle panels) over the normalized amido black signals (left panels). Assays were performed in triplicate.

(**D**) *In vitro* adhesion assays with MRC-5 (n=3) and MDA-MB-231 (n=2) cells treated with ISRIB (0.2 μM) or cycloheximide (50 μg/mL) or left untreated.

Error bars represent the standard deviation. n.s., $p > 0.05$; *, $p \leq 0.05$; **, $p \leq 0.01$; ***, $p \leq 0.001$; ****, $p \leq 0.0001$ by two-tailed *t*-test.

Fig. 3. Identification of the adhesion-related translatome

(**A**) Puromycin immunoprecipitation on extract made from cells treated with either DMSO or 5 mg/mL puromycin for 5 minutes. Extracts were immunoprecipitated using the α-puromycin (clone 12D10) or control IgG antibodies and detected using α-puromycin antibody.

(**B**) Representative α-puromycin (clone 12D10) immunoprecipitation of puromycin-treated steady state and adhering cells (45 minutes post-seeding). As control, we performed the same immunoprecipitation cells that were not treated with puromycin. The extracts shown are representative of the triplicate immunoprecipitation of puromycine treated cells at steady state (fully adhered) and adhering cells (45 minutes post-seeding) used for peptide identification.

(**C**) Log_{10} label-free quantification (LFQ) scores of identified peptides being translated 45 minutes post-seeding compared to those being translated in adhered cells. Selection was based on the level of puromycilated peptides (10X higher) present in each sample , which correspond to actively translated mRNAs. Orange dots represent proteins associated with cellular adhesion, which are presented in the summary table.

Fig. 4. Expression of adhesion-related proteins during cell adhesion

(**A**) Representative detection of levels of translated adhesion-related mRNAs at different time points during cellular adhesion in HeLa cells (left column), in MRC-5 cells (middle column) and MRC-5 cells pretreated with 0.2 μM ISRIB (right column). Experiments were performed in triplicate.

(**B**) Representative detection of levels of translated adhesion-related mRNAs at different time points during cellular adhesion in MDA-MB-468 cells (left column), in MDA-MB-231 cells (middle column) and in MDA-MB-231 cells pretreatedt with 0.2 μM ISRIB (right column). Experiments were performed in triplicate.

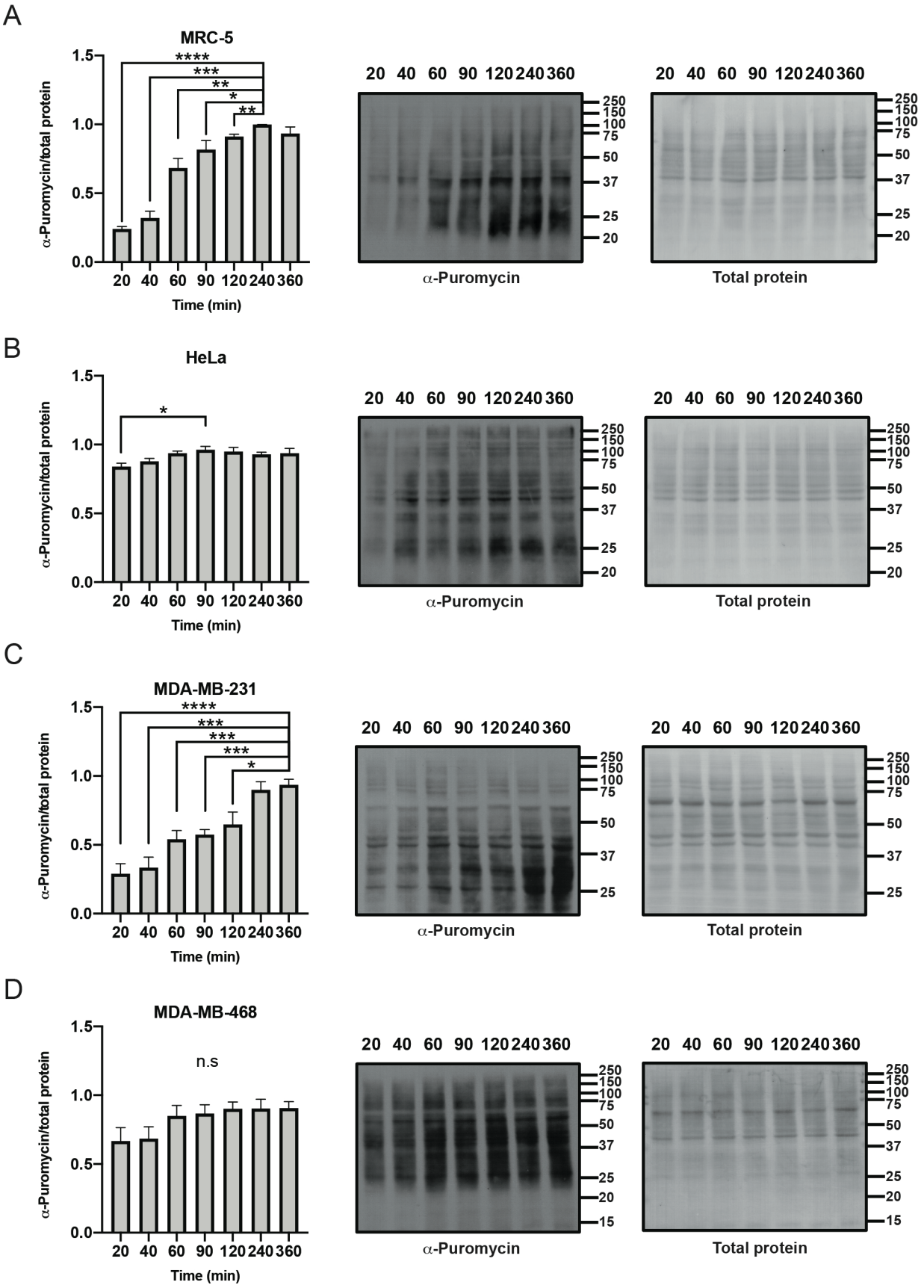

Caillier *et al.* Figure 1

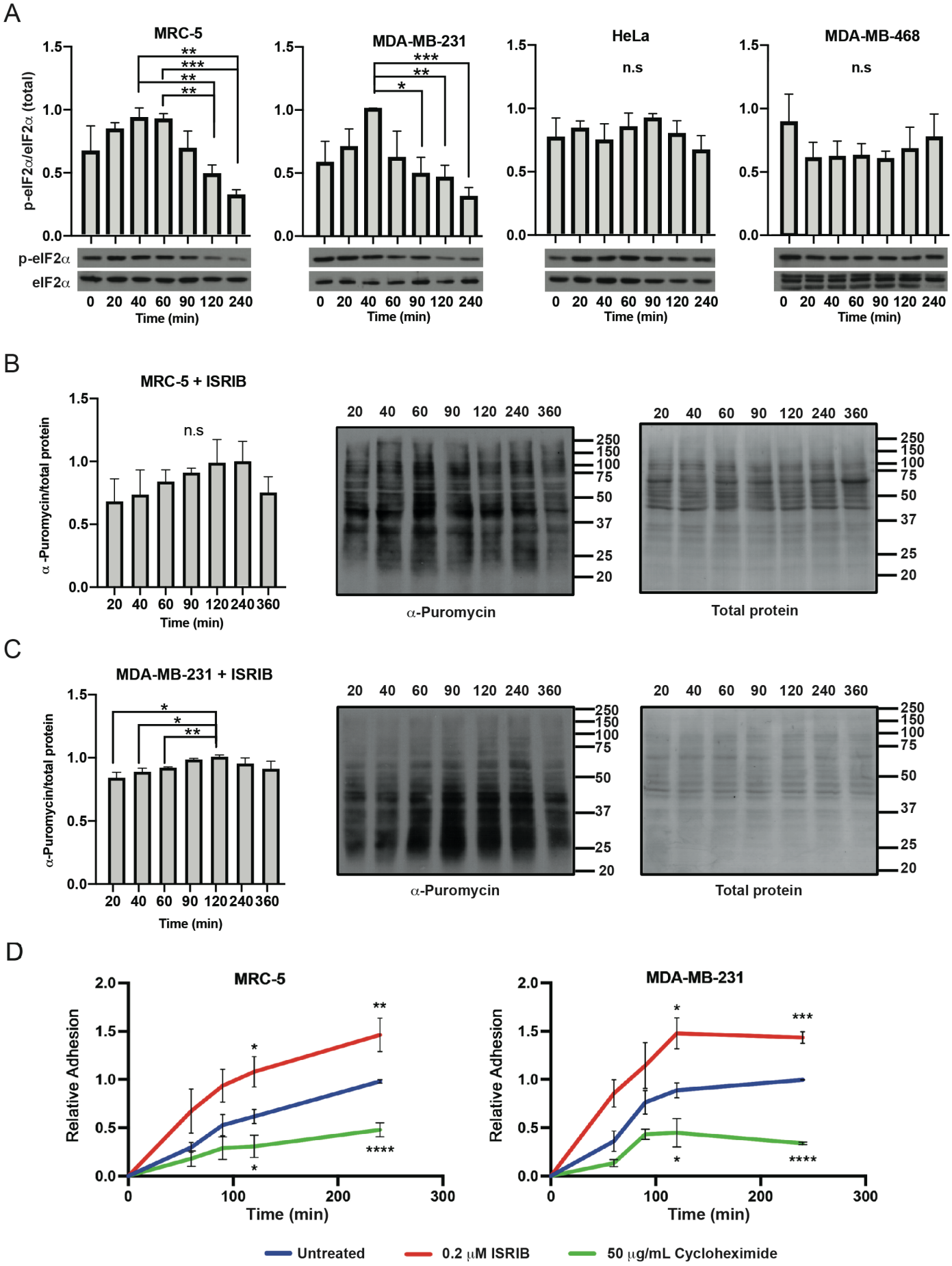

Caillier *et al.* Figure 2

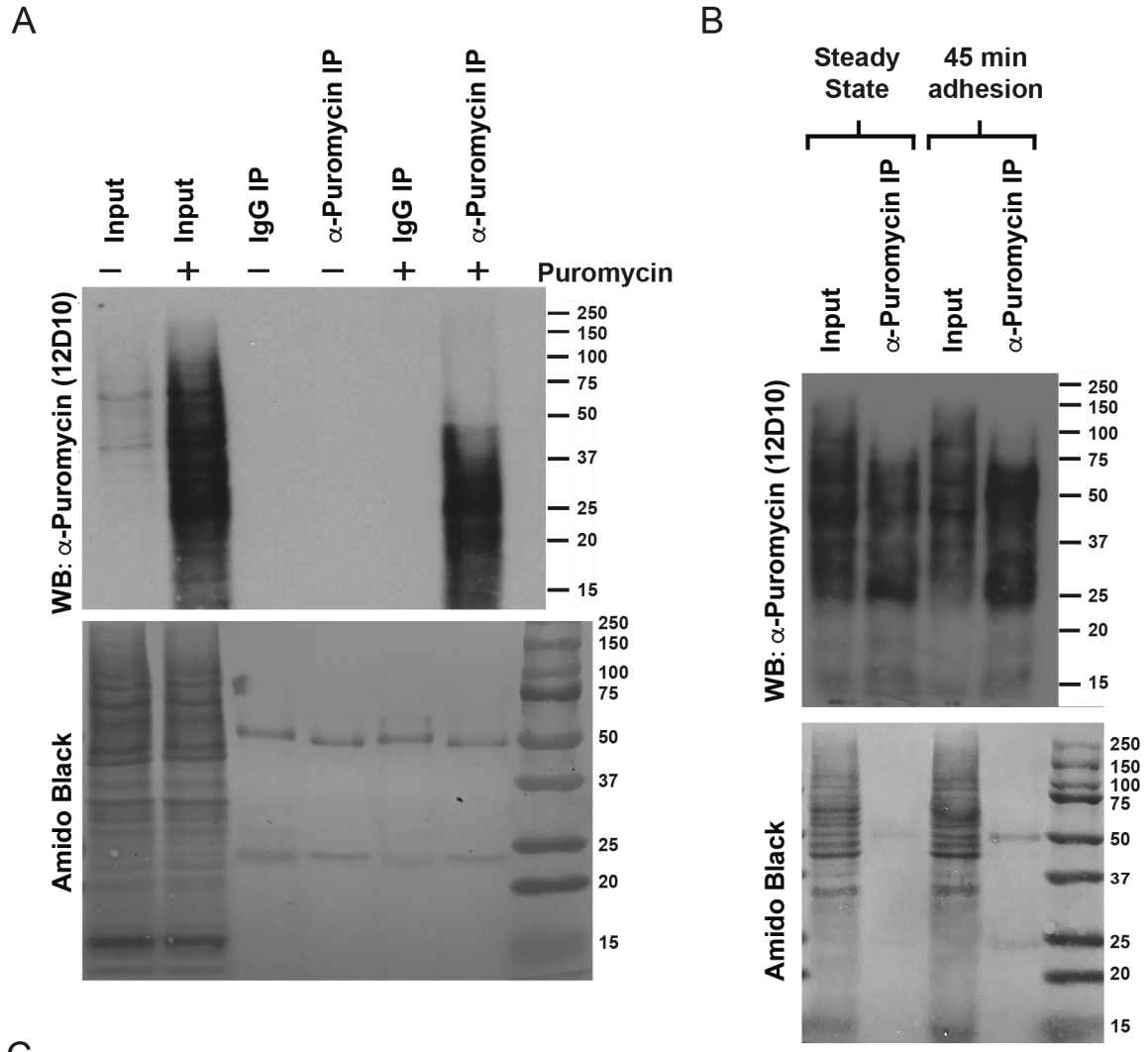

C

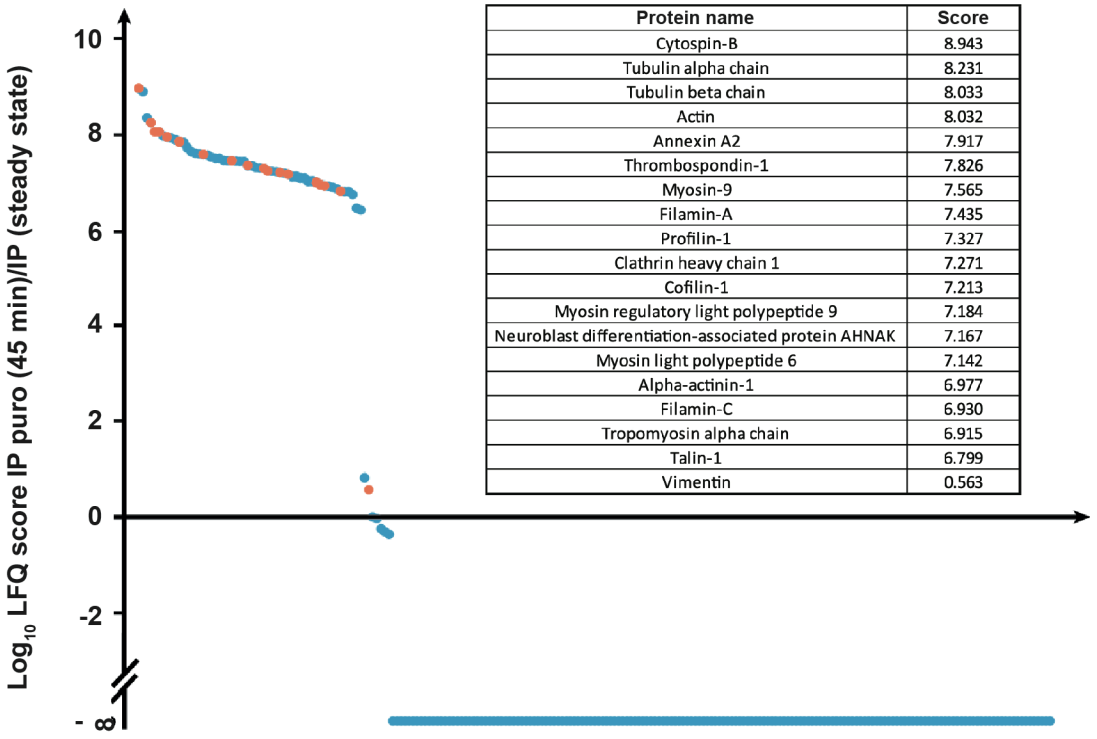

Protein name	Score
Cytospin-B	8.943
Tubulin alpha chain	8.231
Tubulin beta chain	8.033
Actin	8.032
Annexin A2	7.917
Thrombospondin-1	7.826
Myosin-9	7.565
Filamin-A	7.435
Profilin-1	7.327
Clathrin heavy chain 1	7.271
Cofilin-1	7.213
Myosin regulatory light polypeptide 9	7.184
Neuroblast differentiation-associated protein AHNAK	7.167
Myosin light polypeptide 6	7.142
Alpha-actinin-1	6.977
Filamin-C	6.930
Tropomyosin alpha chain	6.915
Talin-1	6.799
Vimentin	0.563

Caillier *et al.* Figure 3

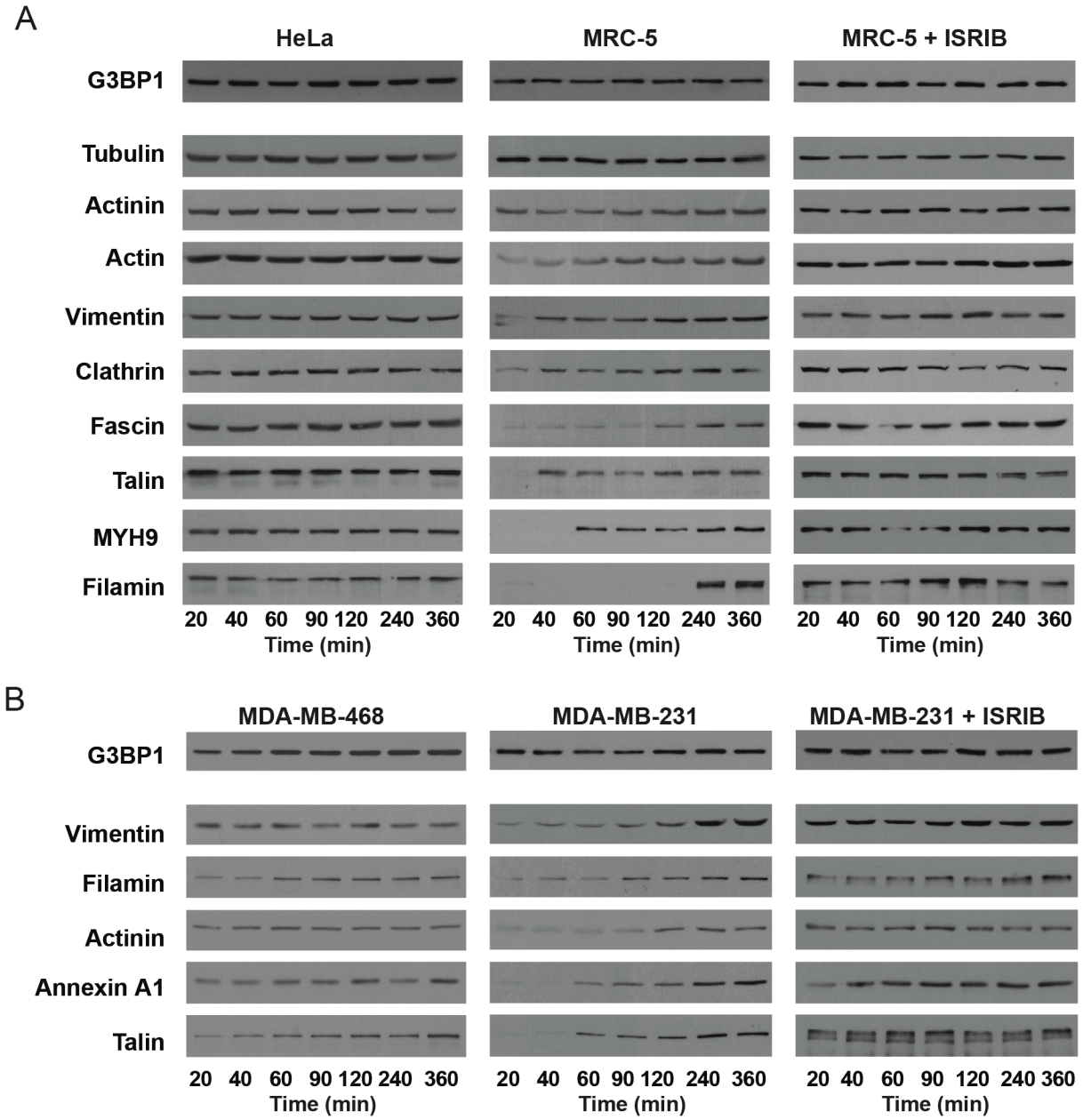

Caillier *et al.* Figure 4